Electronic route to stabilize nanoscale spin textures in itinerant frustrated magnets

Sahinur Reja,[1] Jeroen van den Brink,[1] and Sanjeev Kumar[2]
[1]*Institute for Theoretical Solid State Physics, IFW Dresden, 01171 Dresden, Germany*
[2]*Indian Institute of Science Education and Research (IISER) Mohali, S.A.S. Nagar, Sector 81, Manauli PO 140306, India*
(Received 8 September 2015; revised manuscript received 23 March 2016; published 8 April 2016)

We unveil novel spin textures in an itinerant fermion model on a frustrated triangular lattice in the limit of low electronic density. Using hybrid Monte Carlo simulations on finite clusters we identify two types of nanoscale spin textures in the background of 120° order: (i) a planar ferromagnetic cluster, and (ii) and a noncoplanar cluster with spins oriented perpendicular to the 120° plane. Both these textures lead to localization of the electronic wave functions and are in turn stabilized by the concomitant charge modulations. The noncoplanar spin texture is accompanied by an unusual scalar chirality pattern. A well defined electric charge and magnetic moment associated with these textures allow for their easy manipulation by external electric and magnetic fields—a desirable feature for data storage. We identify a localization-delocalization behavior for electronic wave functions which is unique to frustrated magnets and propose a general framework for stabilizing similar spin textures in spin-charge coupled systems.

DOI: 10.1103/PhysRevB.93.155115

Introduction. Extended magnetic objects that are large enough to be stable against thermal and quantum fluctuations are in common use to densely store information. In materials with immobile magnetic bits, such as for instance patches of magnetization in hard ferromagnets, there are essentially two ways to address individual bits. If one wishes to steer clear of the overhead of wiring each bit individually, the choice that remains is to physically move the storage medium with respect to the reading/writing device. In materials with *mobile* magnetic information carriers the required mechanically moving parts can in principle be avoided by propagating instead the mesoscopic magnetic bits themselves, for instance by applying an electric field in a race-track memory setup [1,2]. In the past years this concept has given a strong impetus to theoretical and experimental research on mobile magnetic textures, such as single magnetic skyrmions, polarons, bubbles, and domain walls [3–11]. On the theoretical side, the focus so far has been on finding novel spin textures in purely magnetic systems. The candidate models are the anisotropic Heisenberg models in the presence of external magnetic field [7,8,12,13].

In this paper, we show that such novel spin textures resembling magnetic polarons can emerge in frustrated antiferromagnets made out of spins and charges on a triangular lattice, which in their phase diagram are close to a region of phase separation. The results are obtained via unbiased Monte Carlo simulations on finite lattices, and crosschecked with variational calculations. We find that ferromagnetic polarons with two different spin orientations are stabilized as a consequence of competing interactions on the frustrated lattice geometry. These spin textures derive their stability from the fact that they appear together with a charge modulation. As opposed to most other magnetic skyrmion and domain-wall textures these spin textures are thus heavily charged and mobile. This implies that they can easily be manipulated with applied electric and magnetic fields, which is a useful feature for data storage. From a fundamental standpoint these results provide a connection between localization physics, frustrated magnetism and novel spin textures. From the charge profiles we infer the presence of an interesting localization to delocalization behavior for electronic wave functions that is specific to frustrated lattices.

Model and Method. The Hamiltonian that we consider consists of localized classical moments Heisenberg-coupled to nearest neighbors and Kondo coupled to itinerant fermions residing on a triangular lattice. The interplay of conduction electrons and the frustrated geometry give rise to many interesting effects, such as for instance a multiple-Q magnetic order [14–18], the anomalous Hall effect [14,16,19,20], coupled spin-charge phases [21–23], and partially disordered phases [24,25]. We work in the limit of strong Kondo coupling and focus explicitly on the low electronic density limit. In the strong coupling limit the electronic spin gets slaved to the local moment and the Kondo model reduces to a double-exchange (DE) model. The resulting Hamiltonian for spinless fermions is given by

$$H = -\sum_{\langle ij\rangle} t_{ij}(c_i^\dagger c_j + \text{H.c.}) + J_{AF}\sum_{\langle ij\rangle} \mathbf{S}_i \cdot \mathbf{S}_j, \qquad (1)$$

where c_i ($c_i^\dagger$) is the electron annihilation (creation) operator with spin parallel to the local magnetic moment $\mathbf{S}_i$. The angular brackets in the summations denote the nn pairs of sites on a triangular lattice. J_{AF} is the strength of the AF coupling between the localized spins. The projected hopping is given by $t_{ij} = t_0[\cos(\theta_i/2)\cos(\theta_j/2) + \sin(\theta_i/2)\sin(\theta_j/2)e^{-i(\phi_i-\phi_j)}]$, where θ_i (ϕ_i) is the polar (azimuthal) angle for localized spins at site i, and t_0 is the bare fermionic hopping amplitude between nn sites. Here onwards we set $t_0 = 1$ as the unit of energy, and therefore the only free parameter in the model is J_{AF}. The model has been extensively studied in the context of colossal magnetoresistance [26–28] and more recently for frustrated itinerant magnets [15,29–31]. It should be noted that the physical scenario described by this model is qualitatively different from that studied in the context of cuprates where doping takes place in the band responsible for magnetism [32].

Here we focus on the limit of very low electronic filling in order to understand the effect of itinerant electrons on a frustrated magnetic state. Note that the DE model alone ($J_{AF} = 0$) leads to a ferromagnetic ground state even for a single itinerant electron. On the other hand, in the absence of electrons the ground state supports a 120° order for all nonzero

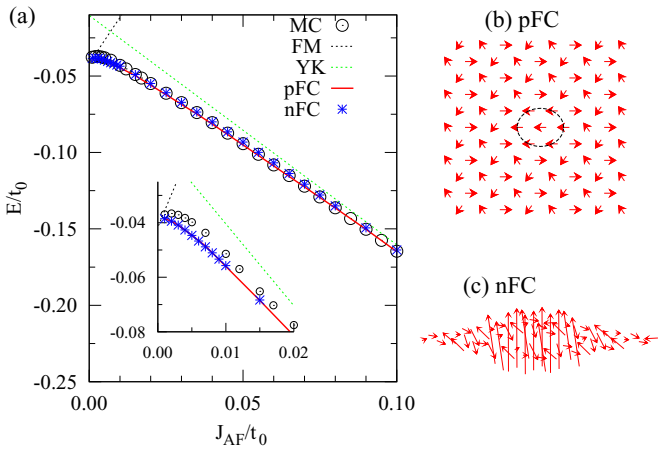

FIG. 1. (a) Total energy per site for different values of J_{AF}. The empty circles are the Monte Carlo results, the solid line is obtained from variational calculations for planar FM cluster (see text), and the star symbols are restricted Monte Carlo simulations where some sites were forced to retain the 120° order. The dashed line with positive (negative) slope represents the energy of a long-range ordered FM (120°) state. Two typical Monte Carlo snapshots showing, (b) a planar FM cluster and (c) A noncoplanar FM cluster, residing in the 120° background.

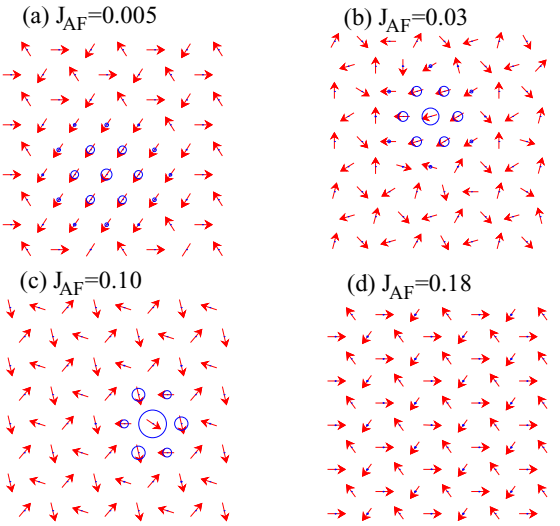

FIG. 2. (a)–(d) Spin and charge configurations at different J_{AF} values as obtained from MC simulations where spins were restricted to remain in a plane. Charge density at a site is represented by the size of the circle drawn on that site. The charge tends to initially localize and then delocalize upon increasing J_{AF} values.

values of J_{AF}. While the overall ground state phase diagrams for this model suggest a tendency towards electronic phase separation in the low-density regime, the detailed real-space nature of the states is not known [33]. In particular, one can ask if certain special spin textures are induced as a consequence of a single electron trying to gain kinetic energy in an otherwise frustrated magnetic structure. In order to find the answer, we make use of a hybrid Monte Carlo method which combines the classical Monte Carlo for spins with numerical diagonalization for fermions [34]. The method is numerically exact, and has served as a very useful tool for exploring the physics of spin-charge coupled systems [35]. The simulations begin at high temperature with a random spin configuration, and the temperature is then decreased in small steps [35]. The results presented here correspond to low temperatures, $k_B T \sim 0.002 t_0$.

Results and Discussions. The total energy per site for the case of one electron on a 12×12 lattice is shown in Fig. 1(a). As expected, the MC energy (circles) interpolates between the FM and the 120° energy asymptotes which are plotted as dashed lines. A careful analysis of the low-temperature real-space spin configurations indicated the presence of two interesting spin-textures in the intermediate J_{AF} regime, $0.01 \leqslant J_{AF} \leqslant 0.05$. The first one is a planar FM cluster (pFC) and the second is a noncoplanar FM cluster (nFC) with additional meron-like texture [see Fig. 1(b) and 1(c)]. These two spin textures are almost degenerate in energy over the entire intermediate J_{AF} range. Note that it is difficult to identify the detailed nature of such textures from a calculation of spin structure factors, as the majority of the background retains the 120° order and therefore the structure factor will be dominated by the 120° state. Taking hints from the textures obtained in the Monte Carlo simulations, we set up restricted Monte Carlo simulations in order to better understand the nature of these spin patterns.

In the first scheme we restrict the spins to lie in a single plane so that the spins are effectively XY type. This can also be thought of as a model for easy plane triangular magnet. The ground state spin and charge configurations obtained from these simulations are shown in Fig. 2. While the large regions of the lattice still follow the 120° pattern, a cluster of aligned spins emerges spontaneously. The charge density is large over these aligned spins, and is essentially zero elsewhere. This provides a simple picture of electronic self-trapping in the 120° background: A single electron tries to make a FM cluster so that it can move freely over this cluster, however there is a price to be paid in terms of the J_{AF}. Therefore, one expects that the size of the FM cluster should decrease upon increasing J_{AF}. Indeed, this is reflected in the real-space plots shown in Fig. 2. However, even though the size of the FM cluster decreases monotonically, the charge patterns indicate a nonmonotonic localization-delocalization crossover. To investigate further the variations of FM cluster size and the charge localization, we perform variational calculations by allowing for FM clusters with different radii, and different orientations w.r.t. the 120° order. This is achieved by orienting all spins inside a ring of radius r in same direction, while the remaining spins retain the 120° pattern. For each value of J_{AF} the FM cluster is varied in radius as well as orientation to obtain the minimum energy. The radius and orientation of the cluster corresponding to the minimum energy state is denoted as r_c and ϕ_c, respectively. The results are plotted in Fig. 3(a). While the radius of the FM cluster decreases monotonically with increasing J_{AF}, the orientation shows a nonmonotonic behavior. $r_c \to \infty$, $\phi_c = 0$ correspond to a FM phase, and $r_c = 0$, $\phi_c = 0$ is the 120° phase. Thus the variational calculation captures naturally the two limiting phases. In the same plot we show the charge at the central site, n_0, of the FM cluster, as a function of J_{AF}. There is

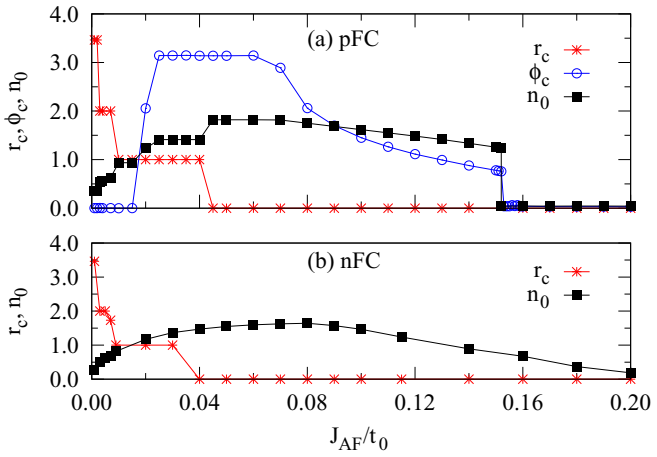

FIG. 3. (a) The radius (red stars) r_c and the angle relative to the 120° state (blue circles) ϕ_c of the planar FC as a function of the AF coupling strength J_{AF}, as obtained from Monte Carlo simulations where spins are restricted to be in a single plane. The filled squares represent the charge density n_0 at the central site of the planar FC. The charge density is scaled up by a factor of 5 in order to clarify the variations. (b) The variation of the radius r_c of the noncoplanar FC and n_0 inferred from a second set of restricted Monte Carlo simulation (see text).

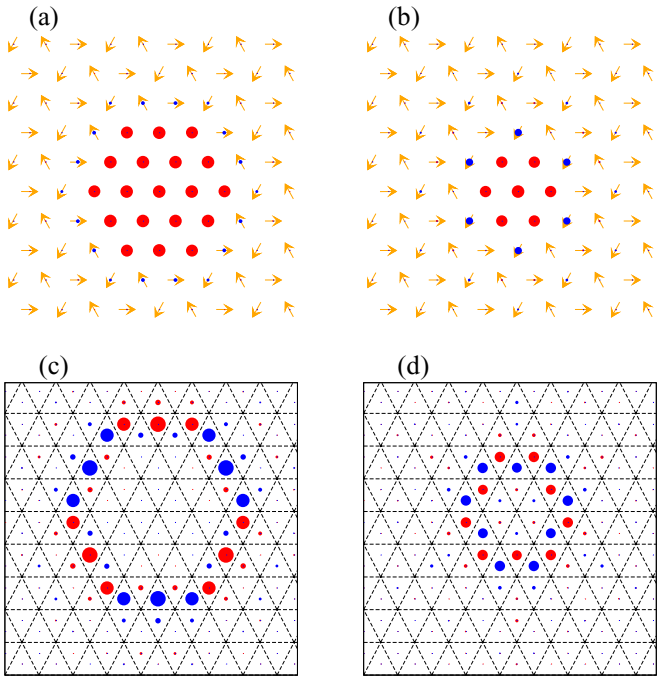

FIG. 4. (a),(b) The noncoplanar spin configuration at $J_{AF} = 0.005$ and $J_{AF} = 0.03$ obtained within restricted MC simulations, where the boundary layers are forced to retain 120° order and a central spin in fixed to be normal to the 120° plane. The magnitude (sign) of $S_z(i)$ is shown as the size (color) of the circles. (c),(d) The scalar chirality pattern for the two values of J_{AF}.

a nonmonotonic variation in n_0 which indicated an interesting localization-delocalization crossover. While the localization is gradual with charge at central site increasing to its maximum possible value around $J_{AF} \sim 0.05$, the delocalization is abrupt near $J_{AF} \sim 0.15$.

As mentioned earlier, another spin texture is almost degenerate in energy with the pFC. This is a noncoplanar spin arrangement where a cluster of spins orients normal to the 120° plane. To analyze this structure and its stability further we perform another set of restricted Monte Carlo simulations. We force the boundary layer of spins to retain the 120° order, and a central spin to point perpendicular to the 120° plane. The remaining spins are updated using the Monte Carlo simulations [35]. The resulting ground state spin configurations are shown in Figs. 4(a) and 4(b) for two values of J_{AF}. Here FM clusters point perpendicular to 120° spin configuration. On the boundary of the FM cluster, z components of the spins on different rings oscillate in sign before they vanish approaching the boundary. The z components of all spins at each site are also shown in panels (a) and (b). The size of the filled circles represent the values of z components and colors (red or blue) represents their sign. The corresponding charge distributions (not shown) are again correlated with the formation of FM clusters. The radius of the noncoplanar FC, together with the density at central site n_0 are shown in Fig. 3(b). Similar to the case of planar FC, the cluster size decreases monotonically upon increasing J_{AF} and the variation in n_0 is nonmonotonic. Note that the nFC texture is not simply a pFC texture rotated by $\pi/2$, but contains interesting modulations of the z components of the spins (see Fig. 4). In order to highlight the noncoplanar character of the nFC texture, we compute the associated chirality patterns. These are shown in Figs. 4(c) and 4(d), where $\chi_{ijk} = \mathbf{S}_i \cdot (\mathbf{S}_j \times \mathbf{S}_k)$ for each triangle with vertices i, j, and k is shown in the center of the triangle. The size of the circle represents the magnitude of the chirality and the color indicates the sign. The positive and negative chiralities are intertwined to result in a zero net chirality. The textures represent examples of localized chirality quadrupoles.

In order to test the stability of these textures in a realistic scenario, it is important to look beyond the single electron case. While a genuine finite-density system would require us to go to larger lattices which is not feasible within the exact simulation scheme, we present results for two electrons on a 12×12 lattice [35]. Figures 5(a) and 5(b) display the ground state spin-charge configuration obtained from the MC simulations with XY spins with two electrons for $J_{AF} = 0.03$ and $J_{AF} = 0.10$, respectively. The spin-charge textures obtained in the one-electron case retain their identity and their separation is determined by the value of J_{AF}. Note that the two pFC textures are not oriented in the same direction when they are adjacent to each other. Consequently, two electrons do not lead to a larger FM patch with uniform charge density, and therefore the results cannot be understood within phase separation scenario. For a better understanding of the two-electron results in terms of single electrons, we study the effective interaction between two pFC textures. This is achieved by assuming a fixed radius for the two pFCs and plotting the total energy as a function of their separation d. The variational calculation also involves an orientation degree of freedom associated with the textures. At each separation the directions of the magnetic moments are varied to achieve the minimum energy [35]. The resulting plots are shown in

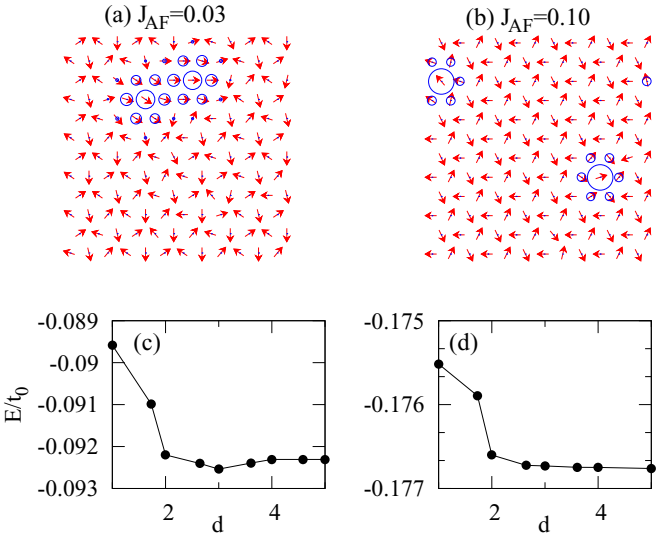

FIG. 5. The spin-charge textures for the case of two electrons for (a) $J_{AF} = 0.03$ and (b) $J_{AF} = 0.1$. Local charge density are denoted by circles as in Fig. 2. (c) Variation of energy with distance d between the centers of the two $r_c = 1$ planar FM cluster for $J_{AF} = 0.03$. (d) Same as (c) for $J_{AF} = 0.1$, where only one spin is deviated from the 120° order.

Fig. 5(c) and 5(d) for the two representative values of J_{AF}. For $J_{AF} = 0.03$, we find that the energy is minimum at a separation of $d = 3$. Indeed, the separation found in the Monte Carlo simulations is close to 3 lattice spacings. For $J_{AF} = 0.10$, the energy keeps decreasing monotonically with increasing d, indicating an effective repulsive interaction between two pFC textures. The Monte Carlo results are consistent with this simple picture, and the two textures reside away from each other [see Fig. 5(b)]. While the effective interaction picture allows for a consistency check for Monte Carlo results, it cannot be used to obtain details of the finite temperature behavior which are contained in the nature of the energy landscape. The complexity of the full energy landscape is also verified by the presence of local minima configurations [35].

In real systems dipolar interactions are likely to be present, therefore we have also studied the stability of these textures in the presence of dipolar interactions (details in Supplemental Material). We find that the pFC is lower in energy in the presence of dipolar interactions. In fact, the textures are stable even when the dipolar interactions are strong enough to influence the 120° order [35]. The long range Coulomb interactions, which have not been accounted for in this study, should further suppress the tendency towards phase separation and favor isolated textures. A remark is in order concerning the generality of such spin-charge textures in Kondo-lattice Hamiltonians. A thermodynamic limit argument suggests that for any finite electronic density inside the phase separation regime, the system will show macroscopic phase coexistence. However, this assumes that the boundary contributions are negligible compared to bulk contributions. This assumption does not hold if the lattice is not infinite or if the volume fraction of one of the phases is much smaller. Therefore, such spin textures can be generally expected if the density lies close to one of the phase separation boundaries in mesoscopic systems.

Conclusion. We show that electronic Hamiltonians involving coupled spin and charge degrees of freedom are capable of stabilizing novel spin-charge textures in the ground state. We study a prototype model for coupled spin and charge degrees of freedom using a numerically exact Monte Carlo simulation method. In the low-density limit, we find that two novel spin-charge textures are stabilized as a consequence of competing interactions on a frustrated lattice. These are the planar FM cluster and the noncoplanar FM clusters, both of which exist together with a localized charge-density profile. We also propose a general scheme for stabilizing such spin textures in electronic Hamiltonians involving coupled spin and charge variables. The search for stable and mobile spin textures in magnetic systems is a rapidly evolving research direction due to the potential applications in data storage devices with easy read/write operations. In contrast to the conventional mechanism of stabilizing novel spin textures in magnetic models, which involves anisotropic interactions, longer-range interactions and external magnetic fields [7,8,12,13], the electronic route presented here can open up new possibilities. Triangular lattice magnets with large spin, such as $LuMnO_3$, $CaCr_2O_4$, etc. are the possible candidates to realize these spin-charge textures [36,37]. The experimental challenge is to introduce a low density of charge carriers in these insulating oxides.

Acknowledgments. This work is supported by SFB 1143 of the Deutsche Forschungsgemeinschaft. S.K. acknowledges hospitality at IFW Dresden during June-July 2015, and support from the Department of Science and Technology (DST), India.

[1] S. S. P. Parkin, M. Hayashi, and L. Thomas, Science **320**, 190 (2008).
[2] U. Bauer, S. Emori, and G. S. D. Beach, Nat. Nanotechnol. **8**, 411 (2013).
[3] W. Jiang, P. Upadhyaya, W. Zhang, G. Yu, M. B. Jungfleisch, F. Y. Fradin, J. E. Pearson, Y. Tserkovnyak, K. L. Wang, O. Heinonen, S. G. E. te Velthuis, and A. Hoffmann, Science (80-.). **349**, 283 (2015).
[4] N. Romming, C. Hanneken, M. Menzel, J. E. Bickel, B. Wolter, K. von Bergmann, A. Kubetzka, and R. Wiesendanger, Science **341**, 636 (2013).
[5] N. Nagaosa and Y. Tokura, Nat. Nanotechnol. **8**, 899 (2013).
[6] S. Seki, X. Z. Yu, S. Ishiwata, and Y. Tokura, Science **336**, 198 (2012).
[7] S. Mühlbauer, B. Binz, F. Jonietz, C. Pfleiderer, A. Rosch, A. Neubauer, R. Georgii, and P. Böni, Science **323**, 915 (2009).
[8] U. K. Rössler, A. N. Bogdanov, and C. Pfleiderer, Nature (London) **442**, 797 (2006).
[9] X. Z. Yu, Y. Onose, N. Kanazawa, J. H. Park, J. H. Han, Y. Matsui, N. Nagaosa, and Y. Tokura, Nature (London) **465**, 901 (2010).

[10] K.-W. Moon, D.-H. Kim, S.-C. Yoo, S.-G. Je, B. S. Chun, W. Kim, B.-C. Min, C. Hwang, and S.-B. Choe, Sci. Rep. **5**, 9166 (2015).
[11] T. Dietl, Nat. Mater. **9**, 965 (2010).
[12] T. Okubo, S. Chung, and H. Kawamura, Phys. Rev. Lett. **108**, 017206 (2012).
[13] A. O. Leonov and M. Mostovoy, Nat. Commun. **6**, 8275 (2015).
[14] I. Martin and C. D. Batista, Phys. Rev. Lett. **101**, 156402 (2008).
[15] S. Kumar and J. van den Brink, Phys. Rev. Lett. **105**, 216405 (2010).
[16] Y. Akagi and Y. Motome, J. Phys. Soc. Jpn. **79**, 083711 (2010).
[17] G.-W. Chern, Phys. Rev. Lett. **105**, 226403 (2010).
[18] S. Hayami and Y. Motome, Phys. Rev. B **90**, 060402 (2014).
[19] H. Ishizuka and Y. Motome, Phys. Rev. B **87**, 081105 (2013).
[20] G.-W. Chern, A. Rahmani, I. Martin, and C. D. Batista, Phys. Rev. B **90**, 241102 (2014).
[21] T. Misawa, J. Yoshitake, and Y. Motome, Phys. Rev. Lett. **110**, 246401 (2013).
[22] S. Reja, R. Ray, J. van den Brink, and S. Kumar, Phys. Rev. B **91**, 140403 (2015).
[23] Y. Akagi and Y. Motome, Phys. Rev. B **91**, 155132 (2015).
[24] H. Ishizuka and Y. Motome, Phys. Rev. Lett. **108**, 257205 (2012).
[25] H. Ishizuka and Y. Motome, Phys. Rev. B **87**, 155156 (2013).
[26] E. Dagotto, T. Hotta, and A. Moreo, Phys. Rep. **344**, 1 (2001).
[27] S. Kumar and P. Majumdar, Phys. Rev. Lett. **96**, 016602 (2006).
[28] C. Şen, G. Alvarez, and E. Dagotto, Phys. Rev. Lett. **98**, 127202 (2007).
[29] J. W. F. Venderbos, M. Daghofer, J. van den Brink, and S. Kumar, Phys. Rev. Lett. **109**, 166405 (2012).
[30] K. Barros, J. W. F. Venderbos, G.-W. Chern, and C. D. Batista, Phys. Rev. B **90**, 245119 (2014).
[31] H. Ishizuka and Y. Motome, Phys. Rev. B **91**, 085110 (2015).
[32] M. Vojta, Phys. Rev. B **59**, 6027 (1999).
[33] Y. Akagi and Y. Motome, J. Phys. Conf. Ser. **320**, 012059 (2011).
[34] S. Yunoki, J. Hu, A. L. Malvezzi, A. Moreo, N. Furukawa, and E. Dagotto, Phys. Rev. Lett. **80**, 845 (1998).
[35] See Supplemental Material at http://link.aps.org/supplemental/10.1103/PhysRevB.93.155115 for further details.
[36] S. Toth, B. Lake, S. A. J. Kimber, O. Pieper, M. Reehuis, A. T. M. N. Islam, O. Zaharko, C. Ritter, A. H. Hill, H. Ryll, K. Kiefer, D. N. Argyriou, and A. J. Williams, Phys. Rev. B **84**, 054452 (2011).
[37] J. Oh, M. D. Le, J. Jeong, J.-h. Lee, H. Woo, W.-Y. Song, T. G. Perring, W. J. L. Buyers, S.-W. Cheong, and J.-G. Park, Phys. Rev. Lett. **111**, 257202 (2013).